Spectroscopic and Electrochemical Study of the Adsorption of $[Co(en)_2Cl_2]Cl$ on γ-Alumina: Influence of the Alumina Ligand on $Co^{(III)/(II)}$ Redox Potential

Vincent Vivier,*,†,‡ François Aguey,† Jeanine Fournier,† Jean-François Lambert,† Fethi Bedioui,§ and Michel Che†,||

Laboratoire de Réactivité de Surface, UMR 7609−CNRS, Université Pierre & Marie Curie, 4 place Jussieu, Casier 178, 75252 Paris Cedex 05, France, Laboratoire Interfaces et Systèmes Electrochimiques, UPR 15−CNRS, Université Pierre & Marie Curie, 4 place Jussieu, 75252 Paris Cedex 05, France, and Laboratoire d'Electrochimie et Chimie Analytique, UMR 7575−CNRS, ENSCP, 11 rue Pierre & Marie Curie, 75231 Paris Cedex 05, France.

Received: August 11, 2005; In Final Form: October 11, 2005

UV−visible and Raman spectroscopies as well as electrochemical techniques have been used to characterize *cis*- and *trans*-$[Co^{(III)}(en)_2Cl_2]Cl$ (en = ethylenediamine) complexes and the γ-alumina-supported *cis*-$Co^{(III)}$ complex. It is shown that the electrochemical reduction of these complexes occurs according to a multistage mechanism involving two electrochemical steps, with the formation of a dimer that was characterized by UV−visible spectroscopy (intervalence band at 670 nm). The apparent standard redox potential for each step has been determined, and experimental results reveal that *cis* and *trans* complexes present similar electrochemical characteristics. It is also shown that the deposition of *trans*-$[Co^{(III)}(en)_2Cl_2]^+$ on γ-alumina leads to an inner-sphere complex (ISC) in a *cis* configuration in which Cl^- ligands are substituted by OH or O^- surface groups of alumina. These changes in the coordination sphere of the complex induce a substantial decrease of its apparent redox potential since it is −0.63 V/SCE (saturated calomel electrode) for the γ-alumina-supported *cis*-$Co^{(III)}$ complex, whereas values of −0.17 and −0.35 V/SCE were determined in dimethyl sulfoxide (DMSO) for the *trans* and *cis* precursor complexes, respectively.

1. Introduction

Many attempts have been made to rationalize the preparation of supported metal catalysts, where the first step is usually the deposition of a precursor of the catalytically active phase, a transition metal complex (TMC), onto an oxide surface. The properties of the final catalyst depend on this deposition step and on the nature of the established TMC/oxide interaction.[1−5] To understand the phenomena that occur during deposition, the concept of interfacial coordination chemistry has been proposed,[6−8] allowing the classification of the adsorption mechanisms of metal complexes on oxide supports.[9] One may distinguish between the following complexes: (a) TMCs, which are electrostatically adsorbed in the diffuse layer and compensate the electric charge of the oxide surface (Figure 1a);[3] (b) outer-sphere complexes (OSCs), where the surface groups of the support enter the solvation sphere of the TMC and interact with the complex by hydrogen bonds or van der Waals forces (Figure 1b);[10] (c) inner-sphere complexes (ISCs), where the surface groups substitute some of the original ligands of the TMC in a ligand-exchange reaction, also called grafting (Figure 1c).[1−5]

In the latter case, the oxide can be considered to be a supermolecular ligand. Since the coordination sphere of the TMC is modified by an inner-sphere interaction, the TMC properties should be significantly altered with respect to those of "free" TMC in solution. Indeed, modifications of spectroscopic properties upon adsorption have been reported and used as evidence for an ISC mechanism.[9] ISC formation should have other consequences, one of the most important of which is a change in the redox properties of the complex. Indeed, it is well-known in the field of "classical" coordination chemistry (i.e., in homogeneous media) that redox potentials of couples involving transition metal complexes depend on the nature of the ligands in the coordination sphere.[11−14] However, very few data are available to assess whether ISC formation does modify the redox potential of grafted TMCs. This may appear surprising since electron-transfer reactions (ETRs) between TMCs in solution have been reported since Taube's pioneering work[15] in many studies at the solid−gas interface.[16,17]

Some attempts have been made to study the electrochemical behavior of oxide-supported species using classical electrochemical techniques on semiconductor electrodes[18−20] or with modified electrodes.[21−23] For the latter, the solid under study (containing the electrochemically active species supported on materials such as zeolites or clays) may be mixed with highly pure graphite to obtain chemically modified working electrodes.[22] The electrochemical response observed with these electrodes is clearly due to the supported species, since it is drastically different in the absence of the solid under study. There is, however, still a lot of debate about the exact nature of the electronic processes involved.[22,23] Moreover, it will be interesting to compare the electrochemical behavior of the initial complex in solution and that of the resulting catalyst at different steps of its synthesis.

Two different approaches can be proposed. The standard redox potential of the grafted complex can be evaluated by the use of successive redox reactions with known potentials. The

* Corresponding Author. E-mail: vivivier@ccr.jussieu.fr.
† Laboratoire de Réactivité de Surface, Université Pierre & Marie Curie.
‡ Laboratoire Interfaces et Systèmes Electrochimiques, Université Pierre & Marie Curie.
§ Laboratoire d'Electrochimie et Chimie Analytique.
|| Institut Universitaire de France.

10.1021/jp058224x CCC: $33.50
Published on Web 12/16/2005

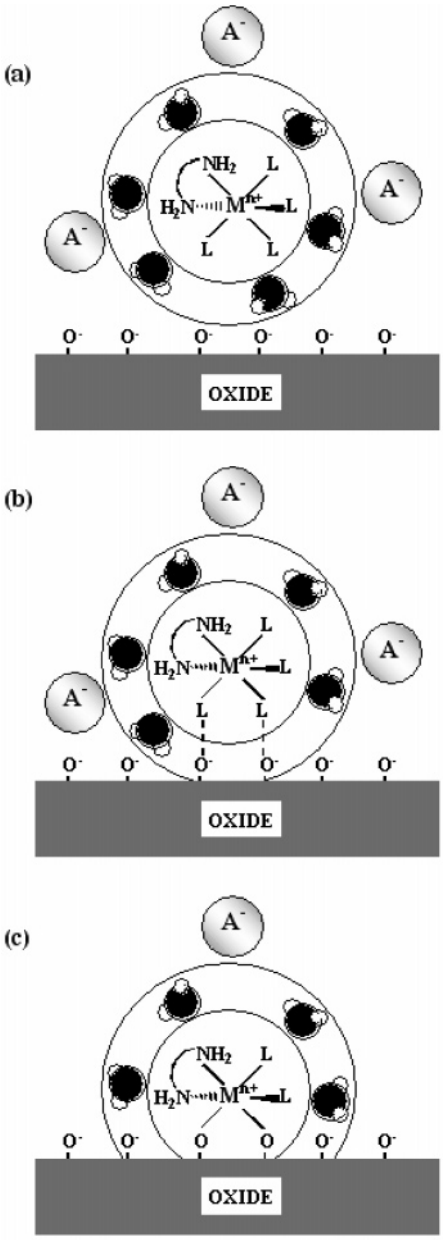

Figure 1. Representation of the various interactions between a TMC and an oxide with the formation (a) of TMCs electrostatically adsorbed, (b) of an OSC, and (c) of an ISC: (M^{n+}) transition metal (III); (L) ligand; (A^-) counter anion.

occurrence of electron transfer can be checked by spectroscopic techniques. For instance, starting with a grafted $Co^{(III)}$ low spin octahedral complex (with two UV−visible bands), its reduction into a $Co^{(II)}$ high spin octahedral complex (with three UV−visible bands) can be readily followed by UV−visible spectroscopy.[24] In this way, it is possible to approach, by trial and error, the value of the standard potential. The second possibility reported here is to take advantage of electrochemical techniques such as cyclic voltammetry.

In the present study, we have selected cobalt complexes because they have been at the basis of Taube's pioneering work on ETRs, and they have also been reported to form ISCs with oxide surfaces.[25,26] Furthermore, they are practically relevant to many catalytic systems.[27,28] Here, we report on (i) the spectroscopic characterization and the electrochemical behavior of the bis-ethylenediaminedichloro cobalt complexes *cis*- and *trans*-$[Co(en)_2Cl_2]Cl$ in solution, (ii) the preparation of a well-defined system by adsorption of the cobalt complex on γ-alumina and the determination of the adsorption mechanism, and (iii) the characterization of its electrochemical behavior, in particular its redox potential, as a function of its adsorption state.

TABLE 1: Elemental Analysis of the Solid $Co^{(III)}$ Reference Complexes and the γ-Alumina-Supported Complex

	%Co	%N	%C	%Cl	%H
theoretical values	20.64	19.63	16.82	37.24	5.65
cis-$[Co(en)_2Cl_2]Cl$	19.18	18.45	15.86	35.34	5.57
trans-$[Co(en)_2Cl_2]Cl$	21.80	17.20	15.67	38.94	5.06
trans-$[Co(en)_2Cl_2]Cl$ deposited on Al_2O_3	0.91	0.70	1.06	0.20	nd[a]

[a] Not determined.

2. Experimental Section

2.1. Synthesis. 2.1.a. *Trans* and *Cis* Precursor Complexes. The *trans*-$[Co(en)_2Cl_2]Cl$ complex (en = ethylenediamine) was synthesized along a previously published procedure.[29] A 25 mL portion of a 1.48 mol·L^{-1} ethylenediamine (en, Acros, 99%) solution was added to 50 mL of an aqueous $CoCl_2$ (Acros, 99.99%) solution (0.6 mol·L^{-1}). The mixture was heated at 100 °C for 1 h under air bubbling. $Co^{(II)}$ was fully converted into $Co^{(III)}$ due to the presence of oxygen from the air atmosphere. Then, 25 mL of hydrochloric acid (HCL, Prolabo, 37%) was added and the resulting solution was heated at 100 °C for 1 h. During the heat treatment, a green crust of small crystals progressively appeared. After slow cooling of the system to room temperature, the obtained green crystals were thoroughly rinsed successively with absolute ethanol (Prolabo, 99.9%) and diethyl ether (SDS, 99.7%). Elemental analysis (Table 1) allowed us to check whether the final product had the composition $[Co(en)_2Cl_2]Cl$, and spectroscopic studies reported in the results section evidenced that the *trans* isomer has indeed been formed.

The *cis*-$[Co(en)_2Cl_2]Cl$ complex was synthesized from the *trans*-$[Co(en)_2Cl_2]Cl$ compound. A 50 mg portion of the *trans*-$[Co(en)_2Cl_2]Cl$ complex was dissolved in 20 mL of distilled water and gently evaporated while the solution was heated at 100 °C. This stage of the synthesis was repeated twice. The residual product was then mixed with very cold water, filtered, and abundantly rinsed successively with absolute ethanol and diethyl ether. The final solid product was pink. Elemental analysis (Table 1) confirmed that it had the same composition as the *trans* isomer, and spectroscopic studies reported in the results section evidenced that it was the *cis* isomer.

The $Co(en)_3Cl_3$ complex was synthesized from 100 mL of a solution of 0.1 mol·L^{-1} $CoCl_2$ containing ethylenediamine (1 mol·L^{-1}) and HCl (1 mol·L^{-1}) under air bubbling (3 h). The mixture was heated at 100 °C until a crust was obtained at the liquid surface. After adding concentrated HCl (15 mL) and absolute ethanol (30 mL), the mixture was cooled to room temperature. The ochre crystals were then thoroughly rinsed with absolute ethanol and diethyl ether, successively.

2.1.b. γ-Alumina-Supported Complex. The γ-alumina-supported Co complex was synthesized via a selective adsorption procedure at room temperature from a *trans*-$[Co^{(III)}(en)_2Cl_2]Cl$ solution. This solution was prepared by adding 2.5 g of the complex salt to 50 mL of distilled water and adjusting the pH to 10 with a concentrated sodium hydroxide solution. A 5 g portion of γ-alumina (Institut Français du Pétrole, ref: Ec 1285, nonporous, 200 $m^2 \cdot g^{-1}$, 150 $\mu m < \phi < 250$ μm) was then suspended in this solution. The mixture was stirred for 4h, then centrifuged, and washed with distilled water until the supernatant

had no visible coloration. The pale-pink solid obtained was dried at room temperature. Elemental analysis of the γ-alumina-supported cobalt complex is reported in Table 1.

With the same protocol, the *cis*-$[Co^{(III)}(en)_2Cl_2]Cl$ precursor was grafted on γ-alumina. A pale-pink solid was also obtained using this isomer as the precursor. Elemental analysis of this solid is similar to that cited in Table 1.

2.2. Spectrometry Measurements. UV−visible spectra were recorded at room temperature on a Cary 5E spectrometer (Varian) equipped with two sources. The first one was a deuterium lamp allowing study the 150−310 nm range, whereas the second one was a tungsten lamp used to study the 310−2500 nm range.

Raman spectra were recorded at room temperature on a Hololab 5000R spectrometer (Kaiser Optical System) with a 785 nm excitation line.

2.3. Electrochemical Measurements. All electrochemical experiments were performed at room temperature under an inert atmosphere (Ar) with a conventional three-electrode cell. The working electrode was either a 2 mm diameter Au-disk or Pt-disk electrode (Tacussel). For the study of the alumina-supported complex, the working electrode was a composite-pressed graphite electrode prepared by pressing 25 mg of graphite powder (Carbone Lorraine, 99.999%) and 25 mg of the solid (alumina-supported complex) on a platinum grid.[22] The reference electrode was a saturated calomel electrode (SCE), and the counter electrode was made of a platinum wire. Both were placed in separate compartments. Cyclic voltammetry measurements were performed with an Autolab PT30 potentiostat (Eco Chemie) equipped with a FRA2 module for electrochemical impedance measurements.

Solutions were freshly prepared with analysis grade solvents [*N*,*N*-dimethyl formamide (DMF, Carlo Erba, 99.8%); dimethyl sulfoxide (DMSO, SDS, 99.5%); and acetonitrile (CH_3CN, BDH, 99.7%)] and deaerated by bubbling with argon gas for 15 min before each experiment. Potassium tetrafluoroborate (KBF_4, Fluka, 97%) was used as an electrolytic salt for all experiments performed in DMF and DMSO.

3. Results and Discussion

3.1. Spectrochemical Characterization. 3.1.a. *Trans* and *Cis* Precursor Complexes. Curves a and b in Figure 2 show the UV−visible spectra of the *cis*- and *trans*-$[Co(en)_2Cl_2]Cl$ complexes in the solid state, respectively. For the latter (curve b), four main transitions are evidenced. The bands at 630 and 460 nm correspond to the allowed d−d transitions of a low-spin d^6 complex in D_{4h} symmetry ($^1A_{1g} \rightarrow {}^1E_g$ and $^1A_{1g} \rightarrow {}^1A_{2g}$, respectively).[30,31] The two bands at 660 and 690 nm are due to spin-forbidden (singlet → triplet) transitions.[32] The spectrum of the *cis*-$[Co(en)_2Cl_2]Cl$ complex (curve a) is characterized by two large bands at 390 and 550 nm, corresponding to the two spin-allowed d−d transitions of a d^6 complex in pseudo-O_h symmetry ($^1A_{1g} \rightarrow {}^1T_{2g}$ and $^1A_{1g} \rightarrow {}^1T_{1g}$).[32]

The Raman spectra of the solid *cis*-$[Co(en)_2Cl_2]Cl$ complex (Figure 3a) and the solid *trans*-$[Co(en)_2Cl_2]Cl$ complex (Figure 3b) exhibit well-defined vibration modes that allow us to distinguish between the two isomers. The characteristic Raman frequencies are reported in Table 2. The two main bands at 282 and 517 cm^{-1} are assigned in both cases to δ(N−Co−N) and ν_s(Co−N), respectively.[34,35] The chlorine−cobalt stretching vibrations are located in the 320−390 cm^{-1} range. A comparison of the spectra permits us to easily distinguish these isomers: particularly the bands at 386, 439, and 458 cm^{-1} for the *cis* isomer (Figure 3a) and the band at 424 cm^{-1} for the *trans* isomer (Figure 3b).

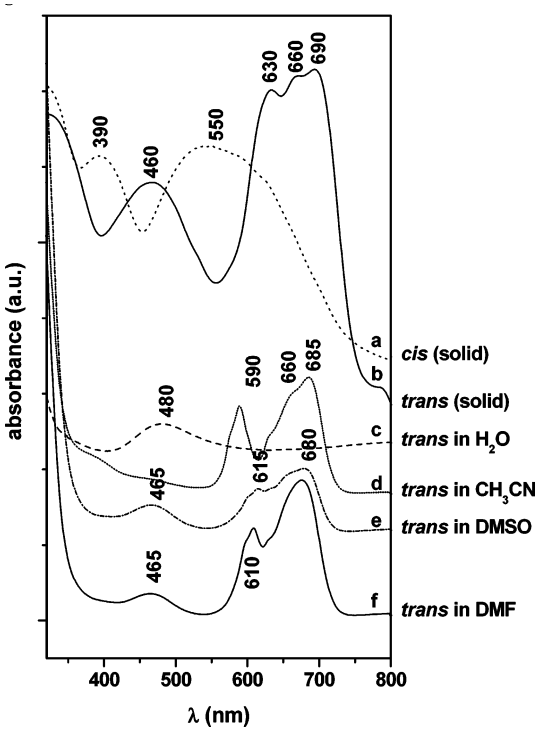

Figure 2. UV−visible spectra of powder materials: (a) *cis*-$[Co(en)_2Cl_2]$-Cl; (b) *trans*-$[Co(en)_2Cl_2]Cl$. UV-visible spectra of *trans*-$[Co(en)_2Cl_2]$-Cl (8 mmol·L^{-1}) in various solvents: (c) distilled water; (d) CH_3CN; (e) DMSO; (f) DMF.

Figure 2 shows the UV−visible spectra of *trans*-$[Co(en)_2Cl_2]$-Cl in different solvents (curves c−f). It appears that, in DMF or DMSO (curves e and f), the main bands (465, 610, and 680 nm) are close to those of the solid compound (Figure 2b). On the other hand, the use of acetonitrile (curve d) induces noticeable band displacements (particularly for the band located at 590 nm) and the disappearance of the transition at 465 nm. In distilled water (curve c), only a single broad band at 480 nm is observed. In these last two solvents, the dissolution of the complex is accompanied by chemical reactions that modify its coordination sphere. Indeed, *cis*- and *trans*-$[Co(en)_2Cl_2]Cl$ can be hydrolyzed.[36] As a result, only DMF and DMSO will be used hereafter for electrochemical studies.

3.1.b. γ-Alumina-Supported Complex. The UV−visible spectra shown in Figure 4 indicate that the adsorbed complex always has the *cis* configuration, although the precursor in solution was either the *cis* or the *trans* isomer.[31] This was also confirmed by Raman spectroscopy (Figure 3c), which evidenced very similar vibration modes to those of the *cis* isomer (Table 2). Measurements at different pH values showed that the amount of adsorbed Co is not straightforwardly correlated to the surface charge of the alumina support and, particularly, remains significant (0.2 wt %) even under pH conditions for which the surface charge is positive (data not shown). That rules out a purely electrostatic adsorption of the complex (Figure 1a). Elemental analysis (see the Experimental Section) of the adsorbed complexes (OSC, Figure 1b; ISC, Figure 1c) reveals the existence of only one ligand per cobalt atom instead of two ligands being present in the precursor complexes. Moreover, it also indicates that little chlorine is coadsorbed, indicating that the formal charge of the adsorbed complex is neutral or at most weakly positive. However, from these data, it is actually not possible to obtain a satisfactory model to describe the formation of these adsorbed complexes.

TABLE 2: Values of Characteristic Frequencies of Raman Spectra for the Solid Reference Complexes *Cis*- and *Trans*-[$Co(en)_2Cl_2$]Cl

	Wavenumber (cm^{-1})			
vibration mode	δ(N−Co−N)[a]	ν(Co−Cl)[a]	ν_{as}(Co−N)[a]	ν_s(Co−N)[a]
cis-[$Co(en)_2Cl_2$]Cl	282	319−350−386	439−458	517
trans-[$Co(en)_2Cl_2$]Cl	251−261−282	334	422	517
supported complex	278	327−389	441−464	521

[a] From refs 34 and 35.

3.2. Electrochemical Characterization. 3.2.a. *Trans* and *Cis* Precursor Complexes. We have first performed the complete electrochemical characterization of the *cis* and *trans* isomers in solution. To the best of our knowledge, although these two complexes have been known for many decades, no work deals with their electrochemical characterization.

The cyclic voltammetry of *trans*-[$Co(en)_2Cl_2$]Cl (2 mmol·L^{-1}) in a DMSO + 0.1 mol·L^{-1} KBF_4 solution is reported on Figure 5a. During the reduction sweep, two cathodic peaks C_1 and C_2 are observed. The first one appears to correspond to a quasi-reversible system and is attributed to the redox couple *trans*-[$Co^{(III)}(en)_2Cl_2]^+$/*trans*-[$Co^{(II)}(en)_2Cl_2$] at ca. −0.17 V/SCE (Table 3). A coulometric study at −0.50 V/SCE shows that this first step involves the exchange of 0.5 electron per complex unit. When applying −0.80 V/SCE, the two steps involve the exchange of 1 electron per complex unit. This suggests that the *trans*-[$Co^{(II)}(en)_2Cl_2$] complex formed during the electrochemical reduction could react with the *trans*-[$Co^{(III)}(en)_2Cl_2]^+$ complex to form a mixed-valence dimer that is reduced at ca. −0.60 V/SCE. This was confirmed by UV−visible spectroscopy performed after each coulometry study (Figure 6).

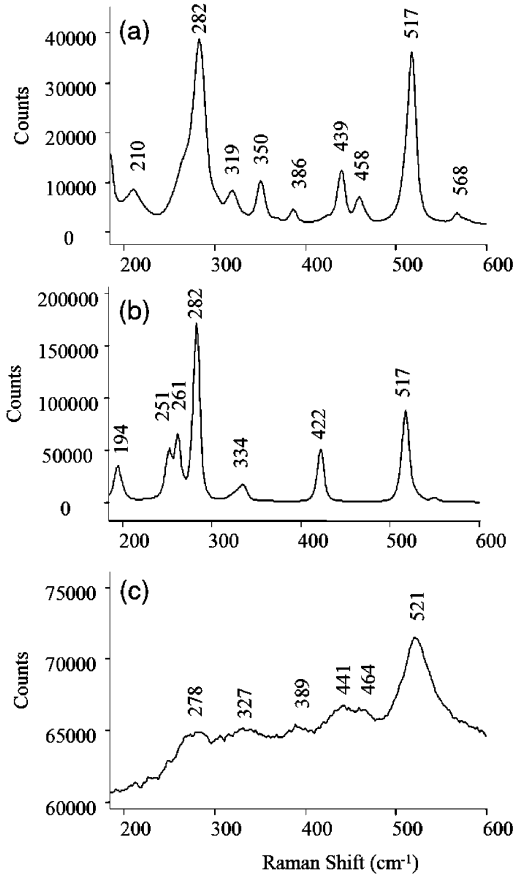

Figure 3. Raman spectra of powder materials (excitation line λ = 785 nm): (a) *cis*-[$Co(en)_2Cl_2$]Cl; (b) *trans*-[$Co(en)_2Cl_2$]Cl; (c) the Co complex adsorbed on γ-alumina.

It is noticeable that, in both cases, the obtained spectra are characteristic of a *cis* configuration. Moreover, an intervalence band located at 670 nm appears after the coulometric reduction at −0.60 V/SCE of the starting *trans*-[$Co^{(III)}(en)_2Cl_2]^+$ solu-

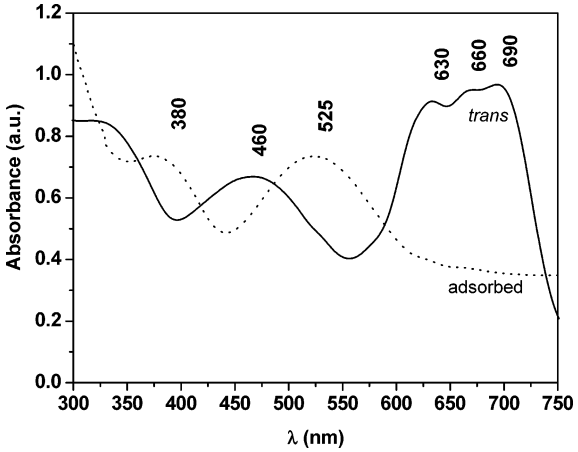

Figure 4. UV−visible spectra of the *trans*-[$Co(en)_2Cl_2$]Cl complex in aqueous solution (solid line) and the Co complex adsorbed on γ-alumina, having a *cis* configuration (dotted line).

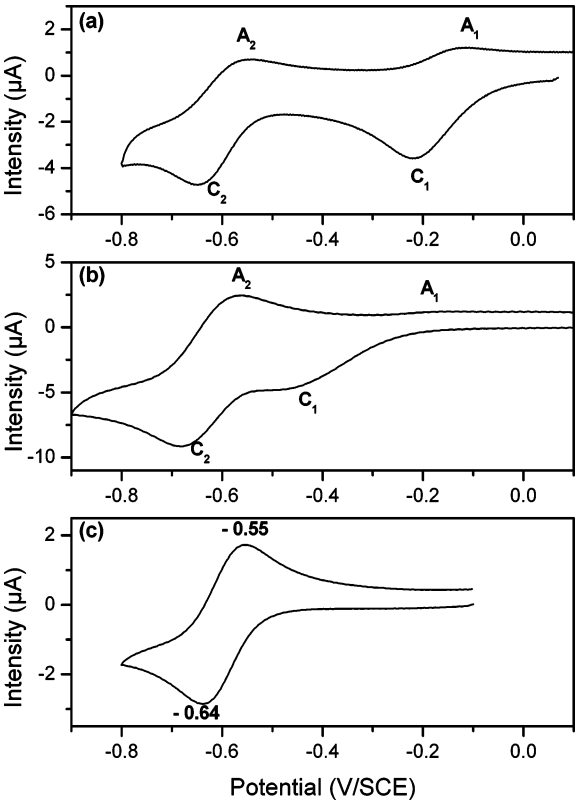

Figure 5. Cyclic voltammograms of (a) *trans*-[$Co(en)_2Cl_2$]Cl (C = 2 mmol·L^{-1}, υ = 100 mV·s^{-1}); (b) *cis*-[$Co(en)_2Cl_2$]Cl (C = 5 mmol·L^{-1}, υ = 50 mV·s^{-1}); (c) [$Co(en)_3$]Cl_3 (C = 1 mmol·L^{-1}, υ = 100 mV·s^{-1}) in DMSO + 0.1 mol·L^{-1} KBF_4 with a 2 mm diameter Au-disk electrode.

TABLE 3: Values of the Apparent Redox Potentials Determined for Complexes in Solution and for the ISC Grafted Complex

	Potential (V/SCE)				
redox couple	*cis*-$[Co(en)_2Cl_2]^{0/+}$	dimer from *cis*-$[Co(en)_2Cl_2]^{0/+}$	*trans*-$[Co(en)_2Cl_2]^{0/+}$	dimer from *trans*-$[Co(en)_2Cl_2]^{0/+}$	ISC grafted complex
DMSO	−0.35	−0.65	−0.17	−0.60	−0.63
DMF	−0.32	−0.62	−0.14	−0.57	nd[a]

[a] Not determined.

tion.[37,38] This is typical of an electronic exchange between two metallic ions of a dimer. Thus, the overall reduction mechanism of the complex in solution can be described as follows:

First electrochemical step

$$trans\text{-}[Co^{(III)}(en)_2Cl_2]^+ + e^- \rightleftarrows trans\text{-}[Co^{(II)}(en)_2Cl_2]^0 \quad \text{at } -0.17 \text{ V/SCE}$$

Conformation change

$$trans\text{-}[Co^{(III)}(en)_2Cl_2]^0 + e^- \rightleftarrows cis\text{-}[Co^{(II)}(en)_2Cl_2]^0$$

Dimer formation (chemical reaction)

$$cis\text{-}[Co^{(II)}(en)_2Cl_2]^0 + trans\text{-}[Co^{(III)}(en)_2Cl_2]^+ \rightarrow [(en)_2Co^{(II)}Cl_2Co^{(III)}(en)_2]^{3+} + 2Cl^-$$

During this step, the configuration of the $Co^{(III)}$ center should change from *trans* to *cis*.

Second electrochemical step

$$[(en)_2Co^{(II)}Cl_2Co^{(III)}(en)_2]^{3+} + e^- \rightleftarrows [(en)_2Co^{(II)}Cl_2Co^{(II)}(en)_2]^{2+} \quad \text{at } -0.60 \text{ V/SCE}$$

The apparent standard potential E^{app} of each step was determined at low scan rates as the mean value between the cathodic and anodic peak potentials. It was found that E^{app}_{DMSO}(*trans*-$[Co(en)_2Cl_2]^{+/0}$) = −0.17 V/SCE and E^{app}_{DMSO}(dimer) = −0.60 V/SCE. However, the electrochemical behavior of the *trans*-$[Co(en)_2Cl_2]^{+/0}$ redox process is greatly influenced by the nature of the electrode materials. On a freshly polished gold electrode and within the first tens of minutes of immersion of the electrode in the electrolytic solution, the anodic peak A_1 located at −0.12 V/SCE disappears and the cathodic peak C_1 shifts toward more negative values to reach −0.30 V/SCE. In contrast, the electrochemical behavior of the dimer remains unchanged. Similar observations were made when using a platinum electrode, whereas, with a carbon electrode, the A_1/C_1 system appears to always be irreversible.

The electrochemical behavior of *cis*-$[Co(en)_2Cl_2]Cl$ in DMSO is shown in Figure 5b and may be contrasted to that of *trans*-$[Co(en)_2Cl_2]Cl$ shown in Figure 5a. In the case of the *cis* isomer, both monomer and dimer reductions occur at more negative potentials than those of the *trans* isomer. The first one is cathodically shifted by about 180 mV (E^{app}_{DMSO}(*cis*-$[Co(en)_2Cl_2]^{+/0}$) = −0.35 V/SCE), and the second one is shifted by about 50 mV (E^{app}_{DMSO}(dimer) = −0.65 V/SCE, Table 3). It should be mentioned that similar voltammetric results are obtained when using DMF as a solvent. The entire voltammogram is then shifted toward more positive potentials of ca. 30 mV, and the apparent standard potentials were determined as

$$E^{app}_{DMF}(trans\text{-}[Co(en)_2Cl_2]^{+/0}) = -0.14 \text{ V/SCE},$$
$$\text{and } E^{app}_{DMF}(\text{dimer}) = -0.57 \text{ V/SCE}$$

Finally, Figure 5c shows the cyclic voltammetry of the Co(en)$_3$ complex in DMSO. It clearly shows a single reversible couple of peaks at −0.60 V/SCE related to the well-known $Co^{(III)}/Co^{(II)}$ redox process.

3.2.b. γ-Alumina-Supported Complex. Figure 7 shows the cyclic voltammograms obtained with the modified electrode containing the raw γ-alumina support (curve a) and the γ-alumina-supported cobalt complex (curve b) in DMSO in the presence of KBF_4 (0.1 mol·L^{-1}). Curve a shows that γ-alumina exhibits no electroactivity. Curve b, obtained with the γ-alumina-supported cobalt complex, exhibits only one well-defined couple of reversible peaks at −0.59 V (reduction) and −0.52 V (oxidation). It is important to note that the intensities of these peaks remain stable for 4 h over repeated cycling.

For reference, we have verified above that the cyclic voltammograms of the precursor, the *trans*-$[Co^{(III)}(en)_2Cl_2]^+$

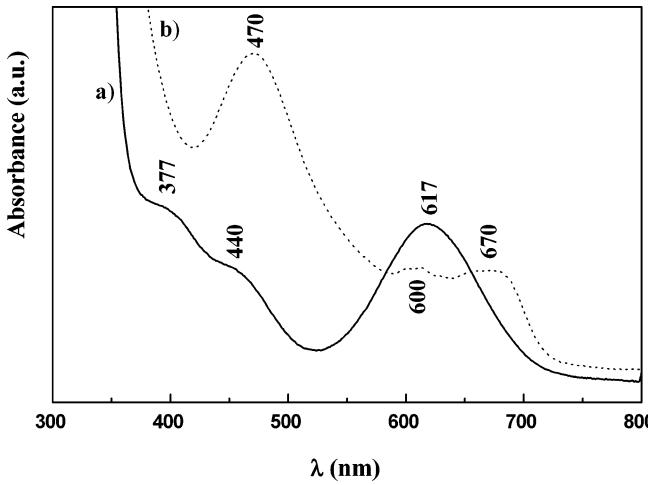

Figure 6. UV−visible spectra of the electrolytic solution containing the *trans*-$[Co(en)_2Cl_2]^+$ complex: (a) before the reduction step; (b) after a reduction step at −0.5 or −0.8 V/SCE.

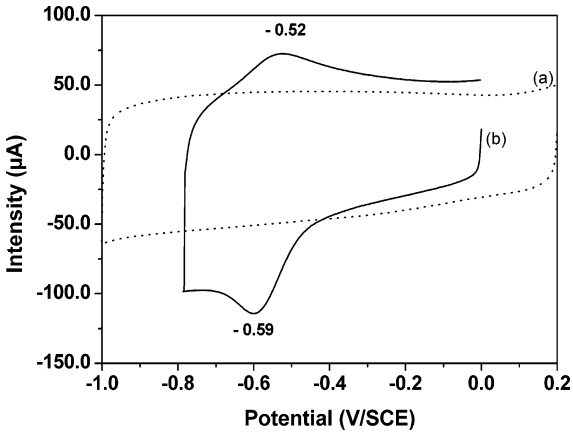

Figure 7. Cyclic voltammograms of the composite-pressed graphite powder electrode in a DMSO + 0.1 mol·L^{-1} KBF_4 solution: (a) containing raw alumina; (b) containing cobalt complexes adsorbed on γ-alumina.

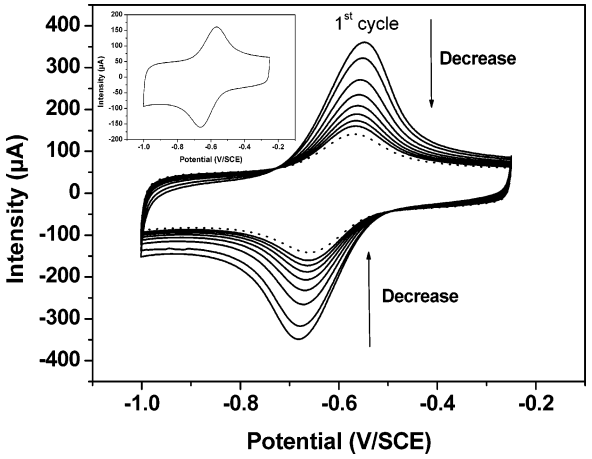

Figure 8. Evolution of the cyclic voltammograms upon adding en to a composite-pressed graphite powder electrode containing cobalt complexes adsorbed on γ-alumina in a DMSO + 0.1 mol·L^{-1} KBF_4 solution. Inset: stable cyclic voltammogram of the composite electrode in a fresh DMSO + 0.1 mol·L^{-1} KBF_4 solution after it has been rinsed and transfered from an en containing solution.

complex, the *cis* isomer, and the corresponding *trans*-diaqua complex (the redox couple is *trans*-$[Co(en)_2(H_2O)_2]^{3+/2+}$; data are not shown for this complex) exhibit in DMSO solution nonreversible cathodic peaks related to the $Co^{(III)}/Co^{(II)}$ reduction at −0.17, −0.29, and −0.11 V/SCE, respectively. These observations allow us to suggest that the reversible redox process for the γ-alumina-supported complex may be related to the $Co^{(III)}/Co^{(II)}$ redox process of OSCs and/or ISCs that are significantly different from all the above complexes.

By adding en ligands to the electrolytic solution, the intensity of the cyclic voltammogram continuously decreased after the first cycle (Figure 8). This loss of electroactivity was accompanied by a pink coloration of the electrolytic solution. This can be explained by the displacement of weakly adsorbed OSCs from the alumina surface to form $[Co^{(III)}(en)_3]^{3+}$ that diffuses in solution far away from the electrode. Elemental analysis and a UV−visible spectrum of the electrolytic solution confirm the formation of the $[Co^{(III)}(en)_3]^{3+}$ complex (data not shown), probably upon substitution of the two OH ligands of the OSC by one en ligand.

Eight hours after the addition of en into the solution, the intensity of the cyclic voltammogram was stabilized. The composite electrode was then thoroughly rinsed and transferred to a fresh DMSO−KBF_4 (0.1 mol·L^{-1}) solution (without en), and the cyclic voltammogram was recorded. It exhibited one well-defined and stable couple of reversible peaks at E^{app} = −0.66 V/SCE (reduction) and −0.58 V/SCE (oxidation) (inset in Figure 8). There was no further evolution in the shape or intensity of the peaks even after repeating scans for 4 h. The fact that no loss of electroactivity occurred after several hours of immersion and/or potential scanning of the electrode in the fresh electrolytic solution means that there was no loss of the redox-active complexes via any chemical or physical process. Indeed, no traces of $[Co^{(III)}(en)_3]^{3+}$ were detectable in solution, at this stage of the experiments. This provides evidence that the observed faradic response does not contain a diffusional component.

Experiments performed with a pressed-powder composite electrode containing γ-alumina and preformed $[Co^{(III)}(en)_3]^{3+}$ complex allow us to rule out the possibility that the electrochemical response may arise from complexes freed from the solid but somehow remaining in the composite electrode. It is likely that no more OSCs are left on the alumina surface after it is transfer into a fresh solution; the couple of peaks observed in Figure 8 (inset) can then be attributed to the $Co^{(III)}/Co^{(II)}$ redox process of the ISC. Therefore, the $Co^{(III)}/Co^{(II)}$ redox process of the ISC can be evaluated to have E^{app} = −0.63 V/SCE.

Comparing this value with those of the precursor complexes in DMSO (for the *trans* isomer, −0.17 V/SCE; for the *cis* isomer, −0.35 V/SCE), it appears that ISC formation has caused a net decrease of the redox potential, which is very close to that of the dimer in solution (E^{app} = −0.60 V/SCE). In other words, the barrier of energy to reduce the compound is much more important when the complex is grafted on alumina than when it is free in solution.

4. Conclusion

The deposition of *trans*-$[Co^{(III)}(en)_2Cl_2]^+$ on γ-alumina leads to an inner-sphere complex (ISC) in a *cis* configuration in which Cl^- ligands are substituted by the OH surface groups of alumina. Neither Cl^- substitution nor *cis/trans* isomerization lead to large enough redox potential shifts of the $Co^{(III)}/Co^{(II)}$ process to account for the effect observed for the alumina supported complex. Therefore, it seems reasonable to interpret the latter effect in terms of the grafting of the precursor complex onto the alumina support. These changes in the coordination sphere of the complex induce a substantial decrease of its redox potential (Table 3), i.e., the oxidized form $Co^{(III)}$ is definitely more stabilized than the reduced form $Co^{(II)}$ upon ISC formation. This might be correlated to the electron-donating properties of the Al−OH ligand; this ligand is expected to be both a σ- and π-donor, especially if it is deprotonated (AlO^-),[6,7] and thus, its interaction should be most favorable with the more highly charged cobalt cation.

The lowering in the redox potential of the ISC (E^{app} = −0.63 V/SCE) should also translate into a significant difference in its reactivity toward redox reactions, compared to that of its free counterpart in solution (E^{app} = −0.17 and −0.35 V/SCE for the *trans* and the *cis* isomer, respectively). These findings are likely to be generalized to other redox couples involving adsorbed transition metal complexes and have obvious implications for the design of supported redox catalysts for liquid-phase reactions.

From a more fundamental point of view, they constitute a first step toward the understanding of electron-transfer reactions at the oxide−solution interface, with potential applications, for instance, in the field of toxicochemistry.[39] The elemental analysis of the adsorbed complex and the redox potential of the ISC in solution seem to show that the ISC presents a complex formulation. However, at this stage of the study, a definitive model of the grafted complex cannot be established and this effort requires further investigations. Finally, the results obtained could help develop a sounder basis for the notion of metal "reducibility" that is often invoked in the preparation of supported metal catalysts.

Acknowledgment. The authors gratefully acknowledge Prof. H. Knözinger and Dr. S. Kuba (Institute of Physical Chemistry, University of Munich, Germany) and J.-M. Kraft (Laboratoire de Réactivité de Surface, Paris, France) for their help in the interpretation of Raman spectra.

Supporting Information Available: Supporting results on the electrochemical impedance spectroscopy characterization of the *trans*-$[Co^{(III)}(en)_2Cl_2]^+$ complex providing more details on the $Co^{(III)}/Co^{(II)}$ redox process. This material is available free of charge via the Internet at http://pubs.acs.org.

References and Notes

(1) Che, M.; Cheng, Z. X.; Louis, C. *J. Am. Chem. Soc.* **1995**, *117*, 2008.
(2) Clause, O.; Kermarec, M.; Villain, F.; Che, M. *J. Am. Chem. Soc.* **1992**, *114*, 4709.
(3) Clause, O.; Carriat, J.-Y.; Che, M.; Kermarec, M.; Verdaguer, M.; Michalowicz, A. *J. Am. Chem. Soc.* **1998**, *120*, 2059.
(4) Carrier, X.; Lambert, J. F.; Che, M. *J. Am. Chem. Soc.* **1997**, *119*, 10137.
(5) Shelimov, B.; Lambert, J. F.; Che, M.; Didillon, B. *J. Am. Chem. Soc.* **1999**, *121*, 545.
(6) Che, M. *Stud. Surf. Sci. Catal.* **1993**, *75A*, 31.
(7) Che, M. *Stud. Surf. Sci. Catal.* **2000**, *130A*, 115.
(8) Lepetit, C.; Che, M. *J. Mol. Catal. A* **1995**, *100*, 147.
(9) Lambert, J. F.; Hoogland, M.; Che, M. *J. Phys. Chem. B* **1997**, *101*, 10347.
(10) Boujday, S.; Lambert, J. F.; Che, M. *J. Phys. Chem. B* **2003**, *107*, 651.
(11) Lappin, G. *Redox Mechanisms in Inorganic Chemistry*; Ellis Horwood Limited: Chichester, England, 1994.
(12) Perrin, D. D. *Rev. Pure Appl. Chem.* **1959**, *9*, 257.
(13) Van Gaal, H. L. M.; Van der Linden, J. G. M. *Coord. Chem. Rev.* **1982**, *47*, 41.
(14) Vlcek, A. A. *Electrochim. Acta* **1968**, *13*, 1063.
(15) Taube, H. *Science* **1984**, *226*, 1028.
(16) Sojka, Z.; Che, M. *J. Phys. Chem.* **1996**, *100*, 14776.
(17) Malka, K.; Aubard, J.; Delamar, M.; Vivier, V.; Che, M.; Louis, C. *J. Phys. Chem. B* **2003**, *107*, 10494.
(18) Haber, J.; Nowak, P.; Stoch, J. *Bull. Pol. Acad. Sci., Chem.* **1997**, *45*, 139.
(19) Haber, J.; Nowak, P. *Langmuir* **1995**, *11*, 1024.
(20) Haber, J.; Nowak, P. *Catal. Lett.* **1994**, *27*, 369.
(21) Walcarius, A. *Anal. Chim. Acta* **1999**, *384*, 1.
(22) Bedioui, F.; Roué, L.; Broit, E.; Devynck, J.; Bell, S. L.; Balkus, K. J., Jr. *J. Electroanal. Chem.* **1994**, *373*, 19.
(23) Bessel, C. A.; Rolinson, D. B. *J. Phys. Chem. B* **1997**, *101*, 1148
(24) Purcell, K. F.; Kotz, J. C. *Inorganic Chemistry*; Holt-Saunders International Editions: Philadelphia, PA, 1977.
(25) Burwell, R. L.; Pearson, R. G.; Haller, G. L.; Tjok, P. B.; Chock, S. P. *Inorg. Chem.* **1965**, *4*, 1123.
(26) Taylor, C. M.; Watton, S. P.; Bryngelson, P. A.; Maroney, M. J. *Inorg. Chem.* **2003**, *42*, 7381.
(27) Schulz, H. *Appl. Catal., A* **1999**, *186*, 3.
(28) Bataille, F.; Mijoin, J.; Lemberton, J. L.; Perot, G.; Berhault, G.; Lacroix, M.; Mauge, F.; Kasztelan, S.; Breysse, M. *Stud. Surf. Sci. Catal.* **2000**, *130C*, 2831.
(29) Bailar J. C. *Inorganic Syntheses*; Frenelius, W. C., Ed.; McGraw-Hill: New York, 1946.
(30) Basolo, F.; Ballhausen, C. J.; Bjerrum, J. *Acta Chem. Scand.* **1955**, *9*, 810.
(31) Csaszar, J. *Acta Chim. Hung.* **1993**, *130*, 639.
(32) Fujita, J.; Shimura, Y. *Bull. Chem. Soc. Jpn.* **1963**, *36*, 1281.
(33) Ban, M.; Csaszar, J. *Acta Chim. Acad. Sci. Hung.* **1968**, *52*, 153.
(34) Chen, Y.; Christensen, D. H.; Sørensen, G. O.; Faurskov Nielsen, O.; Pedersen, E. *J. Mol. Struct.* **1993**, *299*, 61.
(35) Chen, Y.; Christensen, D. H.; Faurskov Nielsen, O.; Pedersen, E. *J. Mol. Struct.* **1993**, *294*, 215.
(36) Aguey, F. Ph.D. Thesis, Université Pierre et Marie Curie, Paris, France, 2000.
(37) Saha, S. B.; Basu, S. *J. Chim. Phys. Phys.—Chim. Biol.* **1970**, *67*, 1520.
(38) Schatz, P. N. *Inorganic Electronic Structure and Spectroscopy, Vol. II Applications and Case Studies*; Salomon, E. I., Lever, A. B. P., Eds.; John Wiley & Sons: New York, 1999; pp 175−226.
(39) Chouchane, S.; Guignard J.; Fournier, J. *Toxicol. Environ. Chem.* **2000**, *75*, 43.